Int J Appl Earth Obs Geoinformation 89 (2020) 102093

Contents lists available at ScienceDirect

Int J Appl Earth Obs Geoinformation

journal homepage: www.elsevier.com/locate/jag

Satellite-derived rainfall thresholds for landslide early warning in Bogowonto Catchment, Central Java, Indonesia

Elias E. Chikalamo[a,*], Olga C. Mavrouli[b], Janneke Ettema[b], Cees J. van Westen[b], Agus S. Muntohar[c], Akhyar Mustofa[d]

[a] Ndata School of Climate and Earth Sciences, Malawi University of Science and Technology, Limbe, P.O. Box 5196, Malawi
[b] Faculty of Geo-Information Science and Earth Observation (ITC), University of Twente, Enschede, 7500 AA, Netherlands
[c] Department of Civil Engineering, Universitas Muhammadiyah Yogyakarta (UMY), Yogyakarta, Indonesia
[d] Balai Litbang Sabo (BALAI SABO), Research Center for Water Resources, Min. of Works and housing, Yogyakarta, Indonesia

ARTICLE INFO

Keywords:
Landslides
Early warning systems
Satellite rainfall products
TRMM
Rainfall thresholds
Antecedent rainfall

ABSTRACT

Satellite rainfall products for landslide early warning prediction have been spotlighted by several researchers, in the last couple of decades. This study investigates the use of TRMM and ERA-Interim data, for the determination of rainfall thresholds and the prediction of precipitation, respectively, to be used for landslide early warning purposes at the Bogowonto catchment, Central Java, Indonesia. A landslide inventory of 218 landslides for the period of 2003–2016 was compiled, and rainfall data were retrieved for the landslide locations, as given by 6 ground stations, TRMM, and ERA-Interim data. First, rainfall data from the three different sources was compared in terms of correlation and extreme precipitation indices. Second, a procedure for the calculation of rainfall thresholds for landslide occurrence was followed consisting of four steps: i) the TRMM-based rainfall data was reconstructed for selected dates and locations characterized by landslide occurrence and non-occurrence; ii) the antecedent daily rainfall was calculated for 3, 5, 10, 15, 20 and 30 days for the selected dates and locations; iii) two-parameter daily rainfall-antecedent rainfall thresholds were calculated for the aforementioned dates; after analysis of the curves the optimum number of antecedent rainfall days was selected; and (iv) empirical rainfall thresholds for landslide occurrence were determined. The procedure was repeated for the entire landslide dataset, differentiating between forested and built-up areas, and between landslide occurrence in four temporal periods, in relation to the monsoon. The results indicated that TRMM performs well for the detection of very heavy precipitation and can be used to indicate the extreme rainfall events that trigger landslides. On the contrary, as ERA-Interim failed to detect those events, its applicability for LEWS remains limited. The 15-day antecedent rainfall was indicated to mostly affect the landslide occurrence in the area. The rainfall thresholds vary for forested and built-up areas, as well as for the beginning, middle and end of the rainy season.

1. Introduction

Rainfall-induced landslides are an important fraction of landslides posing a threat to communities across the globe (Dowling and Santi, 2014; Hong et al., 2007a; Kirschbaum et al., 2009; Rossi et al., 2017; Teja and Dikshit, 2019). There is evidence that higher levels of atmospheric carbon dioxide-induced climate change is resulting in a higher frequency of rainstorms that may trigger landslides (Crozier, 2010; Dowling and Santi, 2014; Gariano and Guzzetti, 2016; Huggel et al., 2011; IPCC, 2014). Coupled with land use changes, population growth and uncontrolled urbanization of hazardous areas have resulted in increasing landslide risk levels (Barla and Antolini, 2016; Brunetti et al., 2018; Gian et al., 2017). The determination of the exact location and time of rainfall-triggered landslide failure is a challenge and measures for reducing the landslide occurrence or for protecting settlements from their destructive impacts can be unfeasibly expensive. In those cases, risk management and the protection of the population can be based on the implementation of early warning systems, that employ precipitation thresholds to mark the potential for landslide occurrence. For this purpose, the most commonly used precipitation indicators are the intensity, duration, and antecedent rainfall (Aleotti, 2004; UNISDR, 2006; BNPB, 2017).

The comprehensive understanding of the slope failure mechanisms and the effect of triggers on it is of paramount significance for

* Corresponding author.
E-mail address: echikalamo@must.ac.mw (E.E. Chikalamo).

https://doi.org/10.1016/j.jag.2020.102093
Received 3 May 2019; Received in revised form 17 February 2020; Accepted 20 February 2020
Available online 27 March 2020
0303-2434/ © 2020 The Authors. Published by Elsevier B.V. This is an open access article under the CC BY-NC-ND license (http://creativecommons.org/licenses/BY-NC-ND/4.0/).

successful landslide forecasting and the development of Landslide Early Warning Systems, LEWS (Uhlemann et al., 2016; Piciullo et al., 2018; Segoni et al., 2018). Various hydrological mechanisms are responsible for changes in the soil pore water conditions that may trigger landslides. These could be snow melting, long duration and low-intensity rainfall, leading to increase of groundwater levels, or short duration and high-intensity rainfall, leading to downwards migration of wetting fronts and changes in pore water pressure (Bogaard and Greco, 2016). Although the trigger is hydrological, most researchers focus on the analysis of rainfall to come up with a probable relationships between occurrence of landslides and rainfall duration and intensity that can be utilized for early warning purposes (Aleotti, 2004; Guzzetti et al., 2008 and 2019; Melillo et al., 2015; Peruccacci et al., 2017; Rosi et al., 2019). Physically-based and empirical models are the major approaches which are used to determine rainfall thresholds for the initiation of slope failures (Guzzetti et al., 2007; Wieczorek and Guzzetti, 2000). Physically or process-based models simulate dynamic processes which occur in a slope before and during a slope failure event by combining hydrological models and slope stability models (Baum and Godt, 2013; Mathew et al., 2014; Melchiorre and Frattini, 2012). They require detailed data on surface and subsurface material properties which are difficult to obtain on a watershed scale (Robbins, 2016), thus limiting their usability to specific slopes or small areas (Rossi et al., 2017). Empirical models, on the other hand, are based on a statistical analysis of the relationship between landslide occurrences and rainfall parameters. They are highly dependent on the completeness of historical landslide inventories, and the temporal and spatial characteristics of the available precipitation data (Robbins, 2016; Tiranti and Rabuffetti, 2010).

Data restrictions are a common issue in developing countries, where landslides often occur in ungauged areas or the number of available rainfall stations is limited. A further issue is the temporal resolution of the data, which is commonly available on a daily rather than hourly basis. To overcome these impediments, satellite-based rainfall estimations may provide an alternative due to their availability, consistency and high temporal resolution (Marra et al., 2014; Robbins, 2016). Currently, there are several products available for satellite-based rainfall measuring and forecast.

The Tropical Rainfall Measuring Mission (TRMM) satellite rainfall product, a joint mission of the National Aeronautics and Space Administration (NASA) and the Japan Aerospace Exploration Agency (JAXA) has been providing rainfall measurements at various temporal and spatial scales since November 1997 up to March 2015 (Kirschbaum et al., 2016; NASA, 2016). The most used rainfall product of TRMM is a daily rainfall estimate at a spatial resolution of 0.25° (~25 km) (Huffman et al., 2010). Since 2015, a more detailed satellite-rainfall product is available in the form of the Global Precipitation Mission (GPM), which was developed by NASA and JAXA. It provides precipitation estimates at a temporal resolution ranging from half hour to monthly and a spatial resolution of 10 km^2 (Hou et al., 2014). Although the GPM product has a higher temporal and spatial resolution, given its short period of functioning up to date, only the TRMM data are suitable for the development of landslide EWS, when landslides inventories prior to the GPM launch are used. ERA-Interim is a global atmospheric reanalysis produced by the European Centre for Medium-Range Weather Forecasts – ECMWF (Berrisford et al., 2011).

The use of satellite rainfall products for LEWS has been spotlighted by several researchers, in the last couple of decades. Early studies conducted by Hong et al. (2006), Hong et al. (2007a,b), Kirschbaum et al. (2009), (2012), Farahmand and Aghakouchak (2013) were amongst the first to use satellite data from TRMM to derive global landslide rainfall thresholds at a small scale of analysis. Liao et al. (2010), worked at the Island of Java, Indonesia, with the NASA TRMM precipitation system and the Weather Research and Forecasting (WRF) rainfall prediction system, and coupled precipitation with physical modeling to successfully back analyse important landslide events. They concluded that satellite data have a great potential for operational early warning, highlighting at the same time spatial and temporal resolution limitations for the study area, as well as the need for further validation with a landslide database. Kirschbaum et al. (2015) demonstrated the use of TRMM and GPM products for regional landslide hazard assessment in Central America and the Caribbean Islands, highlighting the usefulness of satellite-based soil moisture estimates to better quantify the ground conditions prior to extreme rainfall events. However, regarding their use for the establishment of rainfall thresholds for landslide occurrence, there are several limitations, that might lead to an increased rate of either false or missed alarms. An important one is the underestimation of rainfall precipitation, especially for high-intensity rainfalls (Kirschbaum et al., 2009). Another is their low efficiency for measuring convective rainfall patterns (Kidd et al., 2013).

Robbins (2016) addressed the uncertainties in the relationship between rainfall and landslide occurrence, by using a modified Bayesian technique, to produce thresholds of landslide probability associated with rainfall events of specific magnitude and duration, in Papua New Guinea. Rossi et al. (2017), compared the landslides rainfall thresholds derived for the Umbria region, in Italy, either from rain gauges or satellite-derived to find that the latter is lower than the former. Nikolopoulos et al. (2017) based on 10-year rainfall measurements observed large differences between event-based characteristics (described by event duration and magnitude) derived from rain gauge and satellite-based estimates, and for this, they suggested an adjustment of satellite-based estimates for the assessment of the accumulation–duration thresholds. In agreement with that, Brunetti et al. (2018), after comparing the derivatives of four satellite products with ground rain gauges data for developing landslide rainfall thresholds in Italy, they concluded that radar-based rainfall is outmatched by ground data and underestimates rainfall, especially when it is of high intensity. Turkington et al. (2014) developed empirical thresholds for rainfall-triggered debris flows and flash floods using atmospheric indicators for the Ubaye Valley, France, to conclude that for their case study the atmospheric indicators performed better than the weather station thresholds.

Limitations in satellite estimation of peak rainfall events influence the detection of rainfall-triggered landslide events; hence the effectiveness of the intensity-duration relationship is compromised (Kirschbaum et al., 2009; Wu et al., 2012). The limited sampling frequency of satellite data at sub-daily scales restricts their use for the determination of thresholds at shorter intervals (Kirschbaum et al., 2009). Despite their smaller contribution for areas with well-developed and dense rainfall networks, still, they can be an important additional data source in scarcely gauged regions. The satellite-based evalution of rainfall triggered landslides showed the probability of detection ranging from 8% to 60 %. The assessment quality depended on the evaluation period, precipitation data used, and the size of the spatial coverage (Kirschbaum and Stanley, 2018). As most of these studies indicate, to promote the use of satellite derivatives in scarce data areas, analysis has to be performed with different products and extensive landslide inventories, in a variety of morpho-climatic settings, in order to bring into light key aspects for data scaling and uncertainty treatment. This work aims at contributing to this, with the analysis of rainfall thresholds for landslide occurrence at a regional scale, in the Bogowonto catchment, located in central Java, Indonesia.

In Indonesia, rainfall-induced landslides are a widespread and persistent hazard due to ubiquitous landslide conditioning factors such as steep slopes, susceptible soils and high levels of precipitation (Liao et al., 2010). A national-scale landslide risk assessment for Indonesia was carried out by Cepeda et al. (2010) using precipitation data from a network of 149 rain gauges in entire Indonesia and classifying risk (in terms of mortality) as a function of physical exposure, percent forest cover, percent arable land, Human Development Index (HDI), Gender Development Index (GDI), and Human Poverty Index (HPI). Java Island demonstrated a high landslide risk. Indeed, it has experienced many

catastrophic landslide events, moreover due to its high population density in hazardous areas (Hirnawan, 2010; BNPB, 2017). Between the years 1981–2007, an annual average of 49 landslide events with considerable damages was reported for Java island (Liao et al., 2010). Since then, awareness has been raised and has led into the prioritization of the LEWS as the preferred risk reduction measure, since other options such as relocation of exposed communities and engineering measures are less viable (Ngadisih et al., 2017). Local LEWS have been installed in many locations in Java. They mainly consist of monitoring ground displacements or giving an alarm when critical predefined rainfall thresholds are exceeded (Fathani et al., 2011; Karnawati et al., 2009). These are often installed after the occurrence of a landslide event, in order to provide useful warning embedded in local landslide emergency programs supported by the Indonesian National Agency for Disaster Management (BNPB).

Warning systems based on in-situ instrumentation are less effective for large areas due to insufficient instruments to cover all susceptible slopes (Fathani et al., 2008; Sumaryono et al., 2015). To this purpose, and for regional scale analysis, satellite-based rainfall thresholds are being explored in Indonesia. Liao et al. (2010) developed a prototype experimental LEWS for Java island mainly using satellite rainfall estimates. The prototype system which used a physically-based model to predict landslide occurrence had a number of limitations which affected its performance accuracy; one of them is related to the absence of fundamental surface inputs like accurate soil information and field measurements of rain infiltration. The local Administration agency Balai Litbang Sabo (BLS) of the Ministry of Environment is currently developing a LEWS. In this system, rainfall data will be combined with landslide modeling results at the regional and local scale (BLS, 2017). At a regional scale, landslide susceptibility maps will be overlain with rainfall forecasts to identify hazardous areas. At a local scale, physical models will be used to identify possible slope failure location. When fully developed, this warning system will utilize precipitation data from satellite products like TRMM and rainfall forecast ERA-Interim data from the European Centre for Medium Range Weather Forecast ECMWF (BLS, 2017). The work presented in this paper forms part of the ongoing studies for the development of this system.

In particular, the objective of this work is to develop satellite (TRMM) based precipitation thresholds, that can be applied for regional landslide EWS, at the Bogowonto catchment, which is a data-scarce landslide-prone area. Local conditions such as land cover and geology are taken into consideration. The effect of the antecedent rain is analysed as well as the temporal and spatial variability of the thresholds in the study area. The applicability of the thresholds for a landslide early warning using TRMM precipitation data is tested.

2. Study area and data

The Bogowonto catchment, with an area of approximately 600 Km^2, is located in Central Java, Indonesia (Fig. 1). The landscape is characterized by volcanic mountains, with peaks up to 3300 m. The upper part of the catchment is characterized by denudational hills.

Its central part consists of the flatter denudational slopes and floodplains of the Bogowonto river and its main tributary, the Kodil river (Pawestri et al., 2017). The lowest part is dominated by coastal plains and floodplains characterized by flat areas with less than 2 % slope. Geologically, the denudational hills are old volcanic formations of andesite and breccia which have undergone extensive weathering processes (Nugroho et al., 2014). They are mainly composed of reworked materials from the upper units including marls and limestone, while the coastal area is mainly composed of alluvium formation of gravel, sand, and silt.

The area has a tropical climate with a wet monsoon season from October to May, characterized by high-intensity rainfall events and a dry season from June to September (Ngadisih et al., 2017). The average annual precipitation varies from about 3000 mm in the upper catchment to 2500 mm in the lower catchment (Nugroho et al., 2014).

Landslides are frequent in the northern and eastern areas (Fig. 1), with the highest relief, aggravated by strong weathering and fracturing of the geological formations of the upper catchment (Fathani et al., 2008). The central eastern part of the catchment is continuously affected by landslides due to its geomorphic setting coupled with high precipitation amount. Numerous rice fields, houses, and roads are exposed to the landslide hazard. The area is mostly affected by small shallow slides associated with cut slopes in the built up area and only pose danger to few households. There also exist large landslides which can affect small communities most of these are slow moving deep seated landslides. however their (re)activation is not taken into account for the rainfall thresholds which are calculated here.

2.1. Landslide inventory

For this work a landslide inventory was developed based on four sources: i) the BNPB database which records all the reported landslide events; ii), previous studies in the area that focused on specific landslides or events for specific periods (Rusdiyatmoko, 2013; Ulfa, 2017); iii) mass media reports which mostly include events that caused deaths or substantial damage to property, and iv) field mapping.

In total 218 landslides were registered from the sources listed, out of which 167 landslides have a known date of occurrence; they were triggered on 47 different dates. The compiled landslide inventory covers a period of 13 years from 2003 to 2016. Further details such as type of landslide, initiation area and volume are not provided. During field mapping, ubiquitous high tropical trees impeded visual landslide detection, thus it is considered that the inventory might not be complete. Landslides occurring in built up areas are mostly associated with steep cut slopes (Fig. 2).

2.2. Rainfall data retrieval

For the study area, three rainfall dataset sources were used for the early warning system, which are: i) six ground-based rainfall stations with direct rainfall measurements; ii) the Tropical Rainfall Measuring Mission (TRMM) satellite rainfall product, which is an indirect method for rainfall estimation; iii) the ECMWF ERA-Interim rainfall forecast data.

The data from the six rainfall stations in the catchment (Fig. 1) were used as a benchmark to evaluate the performance of TRMM satellite rainfall estimates and modelled ECMWF rainfall forecasts. The rainfall stations provided complete daily rainfall data from 2009 to 2016 and further incomplete measurements for the period 2000–2008. The 3B42 v7 rainfall product of TRMM was used, which is a daily rainfall estimate at a spatial resolution of 0.25° (~25 km) (Huffman et al., 2010). ECMWF data was produced for four periods at 00, 06, 12 and 18 h (UTC) and 2 forecasts per day initialized from analyses at 00 and 12 UTC. The study used ERA-Interim daily rainfall forecast data initialized at 00:00 UTC with a horizontal grid resolution of 0.125°.

3. Rainfall data analysis

Satellite data were compared to ground data for assessing their correlation and for analysing their performance in detecting precipitation extremes.

3.1. Comparison of TRMM and ERA-interim rainfall datasets with ground-based rainfall measurements

Satellite rainfall products have been reported to have limited precision due to random errors, the non-uniform field of view of the sensors that are used and uncertainties in the algorithms for retrieving precipitation measurements (Li et al., 2014). In this work, the reliability of TRMM and ERA-Interim data was assessed by comparison with the

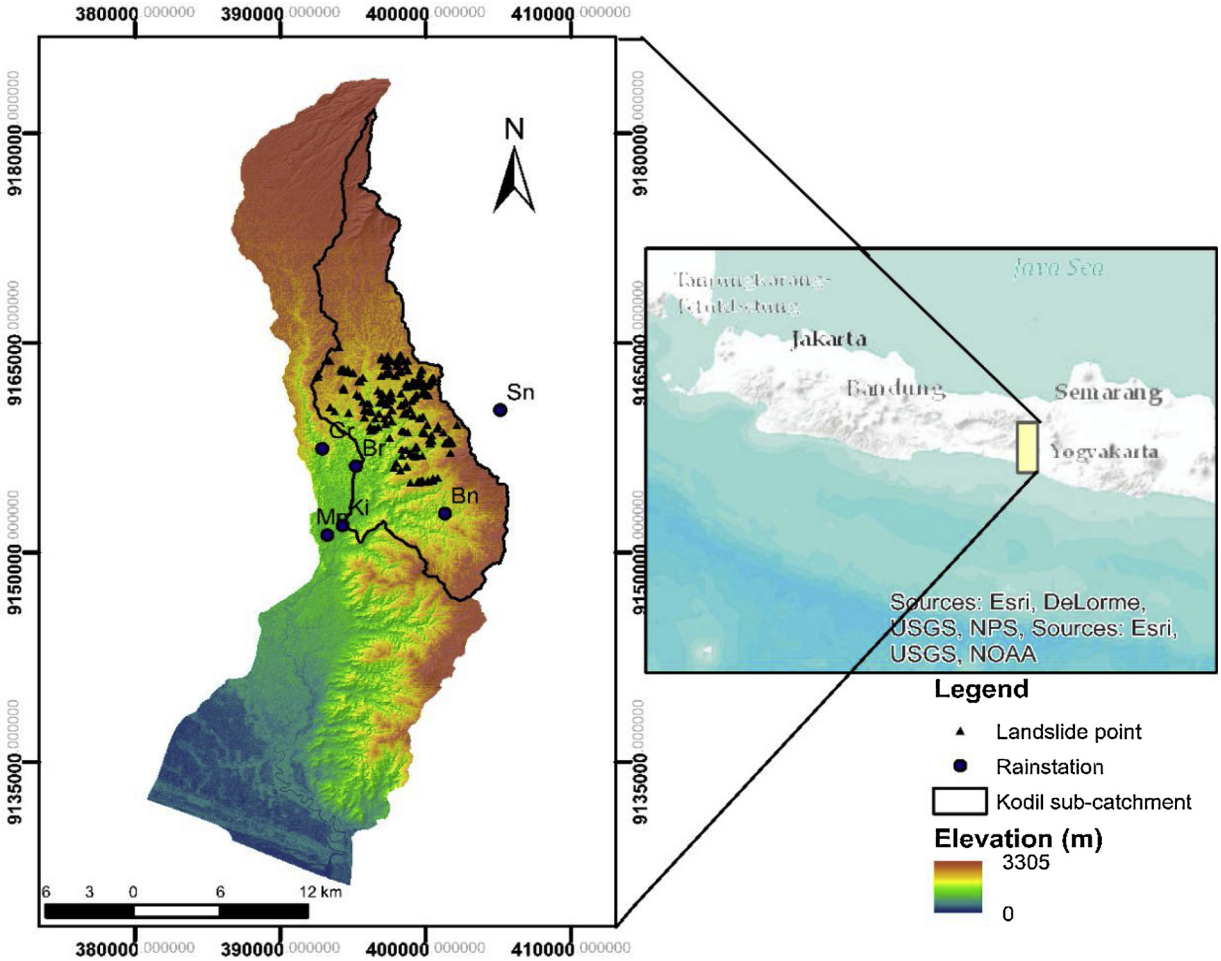

Fig. 1. Map of Bogowonto Catchment. The insert shows the location within Java Island, Indonesia. Rainfall stations: Bener (Br), Banyuasin (Bn), Gentur (Gr), Kedungputri (Ki), Maron (Mn) and Salaman (Sn).

conventional ground-based rainfall measurements using statistical indices such as the correlation coefficient, and the root means square error (RMSE), bias and relative bias values (Li et al., 2014; Wehbe et al., 2017). The formulas for their calculation are given, respectively, by Eqs. (1–4). The correlation was done for the period 2008–2016, with continuous data from the rainfall stations. Satellite rainfall pixels with at least one ground rainfall station were considered in the analysis.

$$R = \frac{\sum_{i=1}^{n}(G_i - \overline{G})(S_i - \overline{S})}{\sqrt{\sum_{i=1}^{n}(G_i - \overline{G})^2}\sqrt{\sum_{i=1}^{n}(S_i - \overline{S})^2}} \quad (1)$$

Where: R: Correlation coefficient, G: gauge rainfall measurements and S: satellite rainfall,

$$RSME = \sqrt{\frac{1}{n}\sum_{i=1}^{n}(S_i - G_i)^2} \quad (2)$$

Where: RMSE: Root Mean Square Error, G: gauge rainfall measurements and S: satellite rainfall,

$$B = \frac{\sum_{i=1}^{n}(S_i - G_i)}{n} \quad (3)$$

Where: B: Bias, G: gauge rainfall measurements and S: satellite rainfall,

Fig. 2. Landslide on cut slopes in the built up area.

Table 1
Results of correlation of daily TRMM satellite rainfall and ERA-Interim rainfall estimates with observed rainfall.

	Daily TRMM	Monthly TRMM	Daily ERA-Interim	Monthly Era-Interim
Correlation Coefficient	0.356	0.831	0.232	0.695
RMSE (mm/day)	23.084	149.619	19.353	135.653
Relative Bias (%)	−28.068	−21.563	19.451	19.439
Bias	−3.016	−56	−19.453	46.266

$$RB = \frac{\sum_{i=1}^{n}(S_i - G_i)}{\sum_{i=1}^{n} G_i} \times 100\% \quad (4)$$

Where: RB: Relative Bias, G: gauge rainfall measurements and S: satellite rainfall.

Table 1 shows the results of the correlation analysis between TRMM rainfall with data from the ground stations, for daily and monthly measurements. For daily rainfall in all stations, there is a low agreement between ground measured rainfall and satellite rainfall estimates as indicated by their low R values. The maximum R value is 0.356 for TRMM. For monthly data, the correlation coefficient is higher and equal to 0.831, which indicates a better correlation between ground and TRMM data. In all cases, TRMM underestimates the rainfall amounts with a relative bias of −28.068 % and −21.563 % for daily and monthly precipitation, respectively. These biases are beyond the limits of −10 % to 10 % for acceptable performance of satellite rainfall products (Tan and Duan, 2017). For ERA-Interim data the correlation with actually measured rainfall data is even weaker, as shown in Table 1.

3.2. Analysis of extreme precipitation indices

Extreme precipitation events have a strong effect on landslide initiation; hence their analysis is essential (Yazid and Humphries, 2015). The quality of both TRMM data for back analysis of the landslide occurrences and ERA-Interim pixel data for landslide forecasting was evaluated in terms of extreme daily precipitation event detection. The satellite estimates and the forecast data were assessed against the ground station data. Extreme rainfall was analysed by using the indices described in Table 2, as provided by the World Meteorological Organisation (WMO) (Tank et al., 2009), and widely used in the literature (e.g., Balling et al., 2016; Rahmani et al., 2016; Yazid and Humphries, 2015).

The calculation of extreme precipitation indices was done for the period from the year 2000–2016, for TRMM and ERA-Interim data. A larger period than for the correlation analysis was chosen to include a higher number of extreme events. The results are summarised in Table 3. They indicate that the number of heavy rainfall days (rainfall ≥ 10 mm) is higher for ERA-Interim (2124 days) followed by TRMM (1381 days) as compared to the actual measured ground station data (1194 days) which can be ascribed to the overestimation of small rainfall events by these products. This overestimation is also reflected in the number of wet days (rainfall ≥ 1 mm) which is high for ERA-Interim (3414 days) followed by TRMM (2525 days) as compared to the station data (2022). On the other hand, the maximum daily rainfall and 5-day maximum rainfall is underestimated by TRMM (183 mm and 257 mm) and ERA-Interim (192 mm and 329 mm) as compared to the measured data (332 mm and 358 mm respectively).

Table 3
Summary of results for extreme precipitation analysis for Station data, TRMM and ERA-Interim rainfall data over the period 2003 to 2016.

Parameter	Station Data	TRMM	ERA-Interim
RX1day	332 mm	182.8 mm	191.3 mm
RX5day	358 mm	256.9 mm	328.5 mm
R10 mm	1194 days	1381 days	2124 days
R20mm	772 days	741 days	521 days
R50mm	223 days	138 days	47 days
SDII	21.9 mm/day	16 mm/day	12.8 mm/day
R95Ptot %	23 %	21 %	18.2 %
R99Ptot %	7%	6%	6.9 %
PRCTOT	44180 mm	40819 mm	43980 mm
Number of wet days (> 1 mm)	2022	2525	3414

4. Procedure for the calculation of rainfall thresholds for landslide occurrence

For the calculation of the rainfall thresholds curves at the Bogowonto catchment, the following steps were considered: i) the TRMM-based rainfall data was reconstructed for selected dates and locations characterized by landslide occurrence and non-occurrence; ii) the antecedent daily rainfall was calculated for 3, 5, 10, 15, 20 and 30 days with respect to the selected dates and locations; iii) two parameter (daily and antecedent rainfall) threshold curves for landslide occurrence were calculated; after analysis of the curves the optimum number of antecedent rainfall days was selected; and (iv) low and high level warning rainfall thresholds for landslide occurrence were established.

The two parameter (daily rainfall and antecedent rainfall) threshold model was selected, considering the lack of sub-daily rainfall data permitting to exploit Intensity-Duration thresholds.

4.1. Reconstruction of rainfall data for landslide occurrence and non-occurrence

The rainfall associated with each one of the landslide events of the inventory was derived by overlaying the landslide location on the

Table 2
Definition of indices used for the analysis of extreme precipitation and how they are calculated. Where RR is daily precipitation amount on a wet day w, W is total number of wet days, k is 5 day interval and j is the length of the period under consideration (adapted from Tank et al., 2009; Yazid and Humphries, 2015).

Indices	Name	Definition	Calculation
RX1day	Daily maximum rainfall	Highest precipitation amount in 1 day	$RX1day_j = \max(RR_{ij})$
RX5day	5 days maximum rainfall	Highest precipitation amount in 5 days	$RX5day_j = \max(RR_{kj})$
R10mm	Number of heavy rainfall days	Count of days when rainfall ≥ 10mm	Count (RR_{ij} ≥ 10 mm)
R20mm	Number of very heavy rainfall	Count of days when rainfall ≥ 20mm	Count (RR_{ij} ≥ 20 mm)
R50mm	Number of extremely heavy rainfall (defined for this study)	Count of days when rainfall ≥ 50mm	Count (RR_{ij} ≥ 50 mm)
SDII	Simple daily intensity index	Mean rainfall when precipitation ≥ 1 mm	$SDII_j$ = sum (RR_{wj}) / W
R95PTOT %	Precipitation due to very wet days	Contribution to precipitation by very wet days	R95Ptot % = Sum if {(RR_{wj} > R95p)/PRCTOT} *100
R99PTOT %	Precipitation due to extremely wet days	Contribution to precipitation by extremely wet days	R99Ptot % = Sum if {(RR_{wj} > R99p)/PRCTOT} *100
PRCTOT	Wet-days (> 1 mm) precipitation total	Total precipitation in wet days	$PRCPTOT_j$ = sum (RR_{wj})

TRMM grid for the reference date and extracting the corresponding daily rainfall. The same procedure was repeated for the daily rainfall preceding the landslide event, for up to 30 days, to obtain the antecedent rainfall. This maximum period was selected based on earlier work in Java of antecedent rainfall and landslide initiation (Hadmoko et al., 2017). Rainfall events of high intensity but with no reported landslides were also extracted from the rainfall database to be used as non-triggering precipitation values, in the determination of landslide rainfall thresholds. To have a meaningful comparison of the triggering and non-triggering rainfall events in the catchment, precipitation data for non-triggering events were selected considering the grids where landslides occurred month(s) after the non-triggering rainfall date. In total, 167 landslides were used that occurred in 47 individual dates between the years 2003 and 2016 and on the other hand 48 rainfall events were selected with the highest rainfall amounts that did not trigger landslides were purposely selected over the same period.

4.2. Incorporation of effective antecedent rainfall

To determine the landslide triggering rainfall thresholds for Bogowonto catchment, we adopted the antecedent daily rainfall model proposed by Glade et al. (2000). The effective antecedent rainfall thresholds in this model are calculated by weighting the antecedent rainfall using Eq. (5) (Glade et al., 2000; Zêzere et al., 2005). The advantage of this approach is that the derived effective antecedent rainfall thresholds can be regarded as a proxy index of soil moisture for the respective days preceding the landslide occurrence day (Glade et al., 2000).

$$AR_x = KP_1 + K^2P_2 + ...+K^nP_n \quad (5)$$

Where AR_x is the weighted effective antecedent rainfall for a day x, P_1 is the daily rainfall for the day before day x, P_n is the daily rainfall for the nth day before day x. K is an empirically derived calibration constant which varies from 0.8 to 0.9 based on the recession of flood hydrographs which is governed by local catchment hydrological characteristics.

For this study, K was assumed to be 0.9 according to the work of Adji and Misqi (2010) where amongst other things they studied the distribution of flood hydrograph recession in Central Java region. This approach roughly takes into account the amount of water that infiltrates into the ground and excludes loss due to overland flow and evapotranspiration, by applying the calibration or decaying constant to all rainfall preceding the landslide day (Ma et al., 2014).

4.3. Evaluation of rainfall thresholds

Several daily rainfall-antecedent rainfall threshold curves were calculated, based on different assumptions, in order to select the most realistic one. Rainfall thresholds were calculated: a) for the entire Bogowonto catchment and all the afore-mentioned rainfall events; b) distinguishing between events on forest and built-up areas; and c) distinguishing between events in four different periods of the rainy season, which extends from October to May: October-November, December-January, February-March, and April-May.

The distinction based on the different land uses was made considering that land cover affects the hydrology of slopes hence has an effect on slope failure. The built-up areas are dominated by cut slopes as a result of the construction of roads, buildings and the growing of crops. The forested areas consist of forests and shrubs and they are generally undisturbed. Of the 166 landslides 107 occurred in forested areas while the remaining 59 in built-up areas.

It was observed that the number of landslides declines as the rainy season advances. For this, the effect of different periods of the rainy season on landslide occurrence and rainfall thresholds was investigated. For the dataset used in this work, the majority of slope instabilities takes place in the months of December to January (79), followed by October to November (42), then February to March (28), and lastly April to May with 19 landslides.

The daily rainfall for landslide occurrence was plotted against 3, 5, 10, 15, 20 and 30-day cumulative antecedent rainfall, to assess the optimal amount of days antecedent rainfall. Non-triggering rainfall events with their respective antecedent rainfall conditions were drawn too. A line was manually fitted to the daily rainfall- antecedent rainfall scatters plot, on the criterion of maximum separation between triggering and non-triggering rainfall events. The optimum number of antecedent rainfall days to consider for the thresholds was selected for the graph on which the fitted line achieved minimum mixing of triggering and non-triggering rainfall values.

4.4. Determination of low and high level warning rainfall thresholds

Rainfall thresholds for two levels of warning, low and high, were derived by adopting the method presented by Zhuang et al. (2014) and Jian et al. (2015). This methodology although not based on rigorous probabilistic analysis of the landslide occurrence data, can provide a general estimate of the expected landslide occurrence, to provide ranked hazard results for the risk management. A line is drawn in the curve that connects the lowest daily rainfall with the lowest cumulative antecedent rainfall that triggered landslides. This line is referred to as the lower envelope of landslides occurrence. As no landslide occurrence has been observed for rainfall lower than this threshold, it is considered to mark a low warning level. A second line referred to as the upper envelope is drawn above the lower envelope crossing the highest rainfall that failed to trigger landslides; this line corresponds to a high warning level.

5. Rainfall threshold results

Fig. 3 shows the rainfall thresholds for the entire Bogowonto catchment, considering 3, 5, 10, 15, 20 and 30 days antecedent rainfall. Minimum mixing of landslide triggering and non-triggering rainfall events is observed from 15 days of antecedent rainfall at least. Thus it implies that there is need for at least 15 days antecedent rainfall or more for landslides to be triggered in the area.

The results suggest that landslides in the catchment are generally initiated when, at least, the cumulative effective 15-day rainfall reaches the lowest threshold of 50 mm and when the daily rainfall is at least 10 mm up to 95 mm. The respective threshold line is given by Eq. (6):

$$y = 0.33x + 80 \quad (6)$$

Following the same criteria, the rainfall thresholds distinguishing between forested and built-up areas were calculated and the critical duration of the antecedent rainfall was selected, accordingly. Fig. 4 shows the respective rainfall thresholds. In the built-up areas the minimum mixing of landslide triggering rainfall events and non-triggering rainfall events is achieved for at least 15 days, while for the forested areas this period is set to 10 days. The proposed rainfall thresholds are given by Eq. (7) for built-up areas, considering 15-day antecedent rainfall and by Eq. (8) for forested areas, considering 10-day antecedent rainfall.

$$y = 0.72x + 77 \quad (7)$$

$$y = 0.83x + 77 \quad (8)$$

Differences in the derived thresholds are potentially related to the water conductivity differences for the two land uses. Under forested areas groundwater may rise faster than in built up areas where soil compaction and paved surfaces dominate, hence rainwater infiltrates at a slower rate as compared to the forested areas.

The different thresholds for events, considering the afore-mentioned four different time periods are shown in Fig. 5. They suggest that landslide occurrence at the beginning of the rainy season (October-

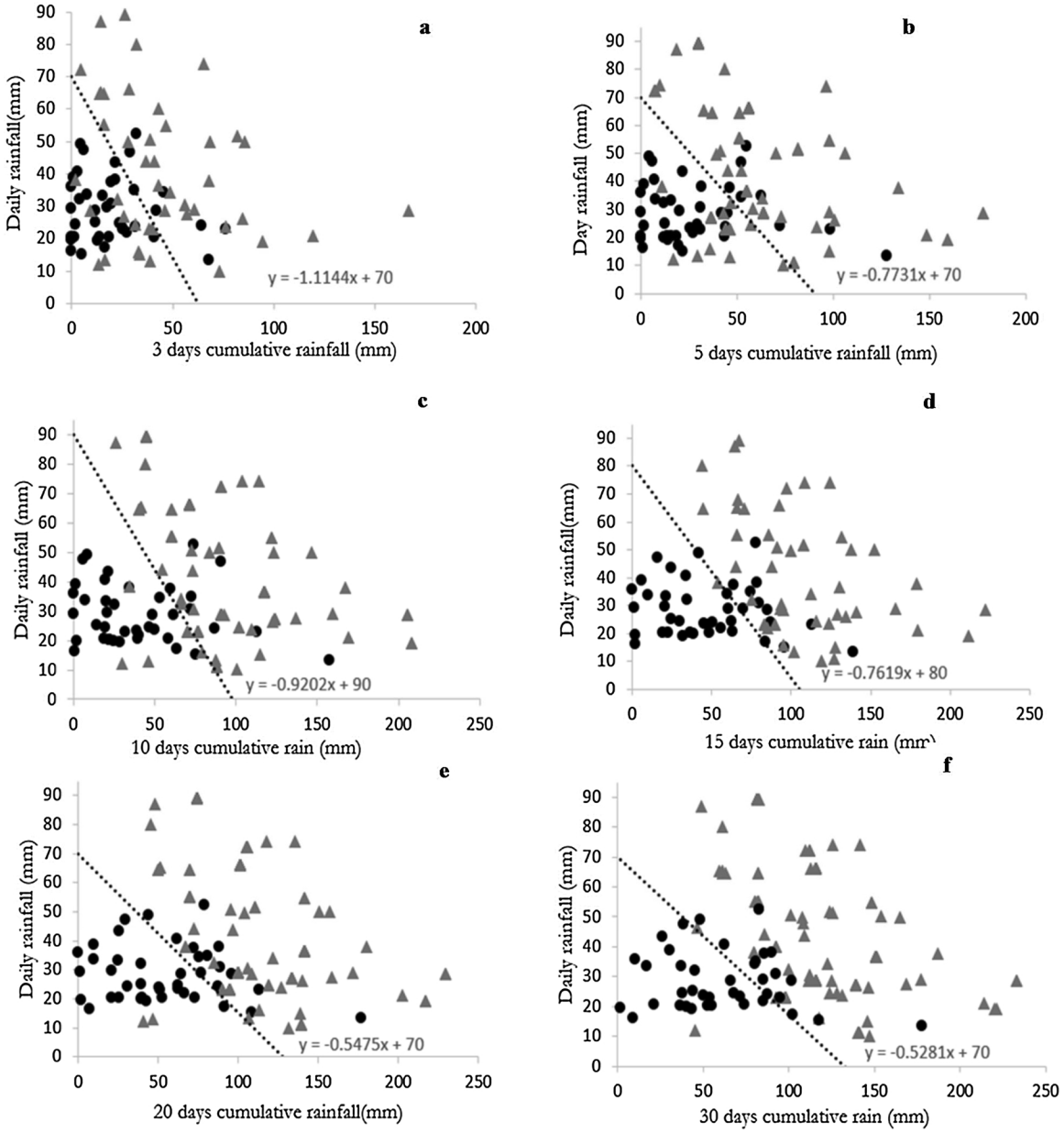

Fig. 3. Scatter plots for daily rainfall against antecedent rainfall for different periods: (a)3 days, (b) 5 days, (c) 10 days, (d) 15 days, (e) 20 days and (f) 30 days. Triangular dots symbolise landslide triggering rainfall events and round dots non-landslide triggering rainfall events.

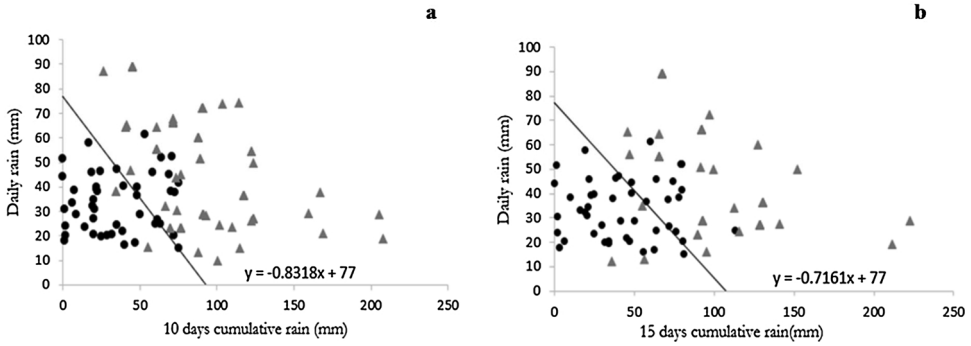

Fig. 4. Scatter plots for determining rainfall thresholds for different land uses: (a) Forest area and (b) built up area. Round dots represent non-triggering rainfall and triangles represent triggering events.

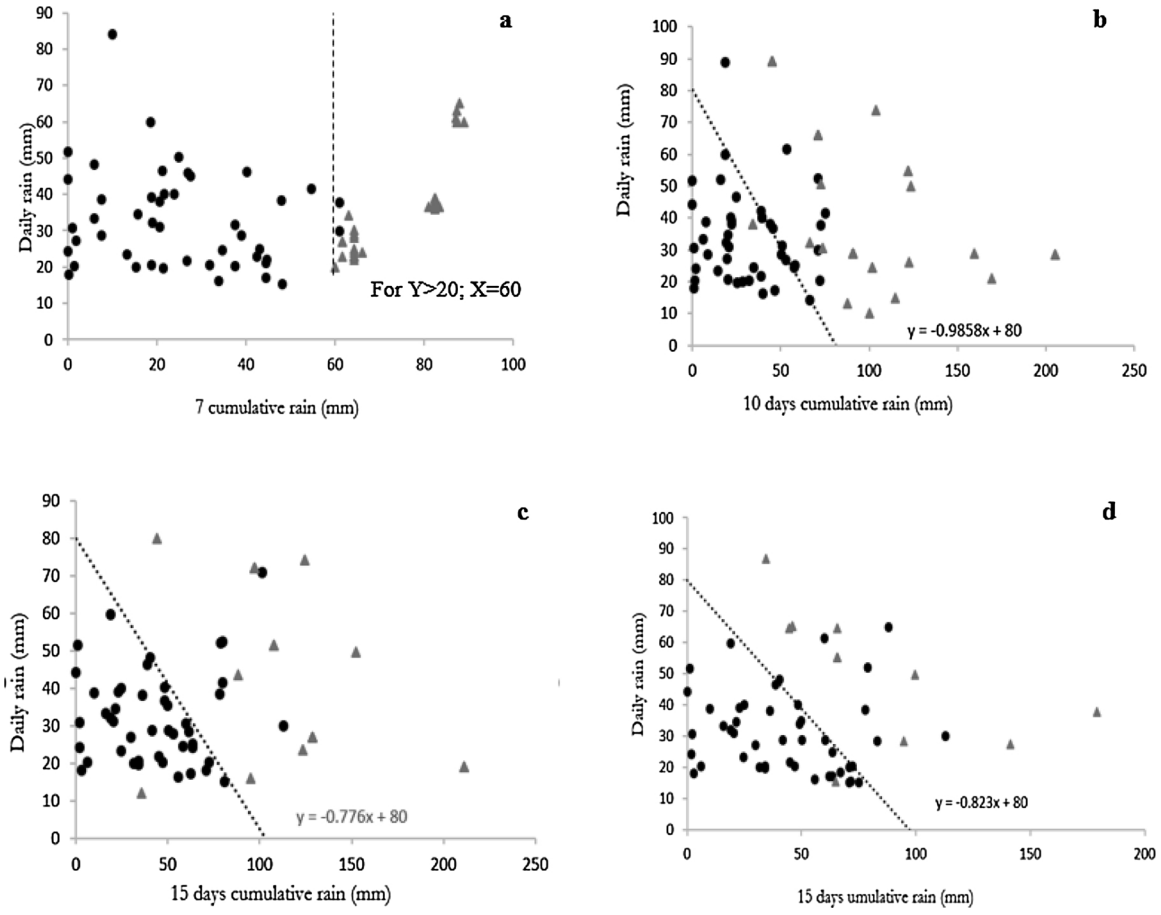

Fig. 5. Graphs for daily rainfall against cumulative antecedent rainfall thresholds for different periods of the rainy season: (a) October to November, (b) December to January, (c) February to March and (d) April to May. Round dots represent non-triggering rainfall and triangles represent triggering rainfall.

November) is mostly influenced by 7 days effective cumulative antecedent rainfall of at least 60 mm, coupled with daily rainfall of at least 20 mm.

For the period December to January, which has the highest number of landslides, the occurrence of landslides in the catchment is associated mostly with 10 days of cumulative rainfall. Lastly, for the periods February to March and the end of the rainy season (April to May), 15 days cumulative antecedent rainfall affect the occurrence of landslides most. Thus, at the beginning of the rainy season landslides occur for relatively lower amounts of antecedent rainfall and relatively higher amounts of rainfall on the event day, as compared to the middle and end of the rainy season, where higher precipitation amounts are required.

All the thresholds derived above were quantitatively evaluated. The evaluation of the thresholds was done based on the following five indices commonly used in the literature (e.g. Begueria, 2006; Lagomarsino et al., 2015; Martelloni et al., 2012):

a) The positive predictive power (PPP) which is the proportion of positive results that are true positives (Beguería, 2006b). Calculated as follows: PPP = TP/ (FP + TP). A perfect classifier would have a score of 1 for PPP.
b) Negative predictive power (NPP) which is the proportion of predicted negatives that are true negatives. NPP = TN/(FN + TN).
c) Sensitivity (true positive rate) which is the proportion of positive cases (landslides) which are correctly classified as such. Sensitivity = TP/(TP + FN).
d) Specificity (true negative rate) which is the proportion of days without landslides which are correctly classified as such. Specificity = TN/(TN + FP).
e) Overall accuracy (Efficiency) which is an index that measures the overall performance of a model by calculating the proportion of correct predictions with respect to the total. Overall Accuracy = (TP + TN)/ (FP + FN + TP + TN) *100.

True positives (TP) are days with landslides correctly detected by the model. True negatives (TN) are days without landslides which the model correctly classified as non-landslide days. False positives (FP) are days which are classified as landslide days but no landslides occurred. Lastly, false negatives (FN) are days with at least a landslide occurrence but the model classified as no landslide day.

The results are shown in Table 4; for thresholds considering different days of antecedent rainfall, the threshold considering 15 days antecedent rainfall has the highest accuracy (86 %). This implies that this threshold can be linked to the early system for landslides in the area. It can be observed in Table 4 that partitioning the thresholds according to landcover and the season of landslide occurrence generally increases the accuracy of the thresholds in predicting landslides, therefore increasing the forecasting effectiveness of the thresholds.

5.1. Low and high level warning rainfall thresholds

The low and high warning level rainfall thresholds were determined as described in Section 4.4. In the resulting graph (Fig. 6), the green line is the lower envelope of rainfall conditions for landslide triggering which call it a low level warning. The red line is the upper envelope, denoting the rainfall for which a higher warning level may be issued.

Table 4
Overall accuracy calculated for the derived rainfall thresholds of Fig. 5.

Rainfall thresholds		Observed						Overall Accuracy (%)
	Predicted	Landslide	No Landslide	PPP (%)	NPP (%)	Sensitivity (%)	Specificity (%)	
3-Day	Landslide	33	8	81	73	73	81	77
	No Landslide	12	33					
5-Day	Landslide	34	7	83	76	76	83	79
	No Landslide	11	34					
10-Day	Landslide	38	8	83	83	84	81	84
	No Landslide	7	33					
15-Day	Landslide	44	11	80	98	98	73	86
	No Landslide	1	30					
20-Day	Landslide	43	14	75	93	96	66	81
	No Landslide	2	27					
30-Day	Landslide	44	13	77	97	98	68	82
	No Landslide	1	28					
Forested Area	Landslide	37	12	76	94	95	74	84
	No Landslide	2	34					
Built up area	Landslide	21	14	60	91	88	71	76
	No Landslide	3	32					
Seasonal Oct- Nov	Landslide	23	2	92	100	100	96	97
	No Landslide	0	44					
Seasonal Dec-Jan	Landslide	17	6	74	97	94	84	88
	No Landslide	1	32					
Seasonal Feb-Mar	Landslide	10	6	63	98	91	87	88
	No Landslide	1	40					
Seasonal Apr-May	Landslide	9	6	60	98	90	87	88
	No Landslide	1	40					

6. Discussion

Comparison of TRMM rainfall estimates and ERA-Interim rainfall forecast data with the observed rainfall from meteo stations has indicated that these products generally underestimate rainfall up to 30 % for both daily and monthly rainfall in the study area. A possible reason for this poor performance is the coarse resolution of the rainfall products grid (25 km for TRMM) on which the point measurements with the station data were overlain. Coarser grids demonstrate a smoothening effect on the spatial variability of rainfall, thus leading to a low correlation with the ground observations, in case of local peaks. For the TRMM monthly rainfall, the respective correlation was better (0.83) as the local effects are less pronounced. Better performance might be attributed to the improved calibration of the models used to derive monthly rainfall as compared to daily rainfall (Toté et al., 2015). For the ERA-Interim rainfall forecasts, the lack of agreement with observed rainfall could be attributed to uncertainties related to the parameterization of convection (Bumke, 2016).

The effect of spatial resolution is also important here, given that for a grid of 80 km, spatially heterogeneous rainfall patterns cannot be depicted well. Thus, the use of satellite products for identifying local rainfall extremes is restricted. The analysis of extreme rainfall using satellite datasets shows that ERA-interim overestimates the number of wet days, but the total amount of precipitation is very similar to the observed rainfall for the period 2003 to 2016. TRMM indicates a larger number of days with very heavy and extremely heavy precipitation as compared to ERA-Interim; thus it detects better high rainfall events. For 1 and 5-day maximum rainfall and days with heavy precipitation, ERA-Interim forecasts outperform TRMM estimates. Nevertheless, ERA-Interim forecasts underestimate the days with heavy and extremely heavy precipitation.

As TRMM performs well for the detection of very heavy precipitation (see Table 3 for R20 mm), it can be used to indicate the extreme rainfall events that often are triggers for landslides. On the contrary, as ERA-Interim failed to detect those events, its applicability for LEWS remains limited, for the studied catchment. Bias correction of the product data could be a solution to this however this is beyond the scope of this paper.

Therefore, using the TRMM satellite rainfall product, landslides in Bogowonto catchment have been empirically correlated with weighted antecedent rainfall conditions by taking daily rainfall as dependent variable and different periods of antecedent rainfall as independent variable. Following this analysis, at least 15 days antecedent rainfall conditions and daily rainfall on the landslide event day has been found to be correlated to the occurrence of landslides in the study area. The weighted thresholds are preferable because they reduce mixing of

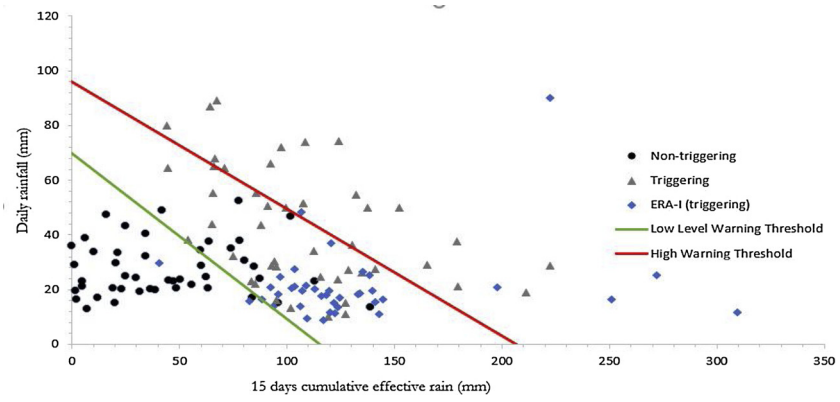

Fig. 6. Plot for 15 days effective antecedent rainfall and daily rainfall: black dots symbolise non-landslide triggering rainfall events and triangular dots symbolise landslide triggering rainfall events, using TRMM data. The respective EAR-I data for triggered landslides are printed in blue (For interpretation of the references to colour in this figure legend, the reader is referred to the web version of this article).

landslide days from non-landslide days as they make rainfall occurring more days before the event days to be less important as compared to rainfall in days close to the event.

The relationship between rainfall and landslides occurrence is not straight forwared, as evidenced by the non-occurrence of landslides when the conditions that triggered landslides in the past are reached or exceeded. This inherent uncertainty can be partly dealt with when the determination of thresholds is probability-based (Berti et al., 2012).

In the proposed method, the manual fitting of the proposed rainfall thresholds to the data is a shortcoming entailing uncertainties which can be minimized using regression analysis. This was out of the scope of the research presented in this paper; however this improvement is strongly needed and it will be developed in future research activities.

Transferring the thresholds to other areas may lead to poor results due to spatial variability of rainfall and differences in hydrological, geomorphological and geological characteristics of catchments. In addition, the derived thresholds may be an underestimation as they have been determined using TRMM rainfall estimates which underestimate rainfall. Lastly, we did not have enough data to derive different rainfall thresholds related to different types of landslides, although it has been shown elsewhere that the effect of antecedent precipitation differs based on various landslide types for example deep seated and shallow landslides (e.g. Muntohar, 2008; Zêzere et al., 2005)

7. Conclusions

For the study area, the results indicated that it is possible to use TRMM data to determine rainfall thresholds that can be used in a landslide EWS, considering daily and antecedent rainfall. We conclude that TRMM data performed reasonably well for the detection of heavy precipitation, thus it can be efficiently used to indicate extreme rainfall events that trigger landslides. However, the use of TRMM-based data leads to lower rainfall thresholds than based on the measured rainfall data from rain gauges, thus the two sets of data cannot be combined in the same system. The thresholds developed using the TRMM data are still only suitable for now-casting, with information of rainfall on the day of occurrence. The mixing of TRMM data with ERA-Interim data for forecasting daily rainfall, as an essential component of LEWS, has been proven to be problematic in the study area.

For the study area and the recorded landslide events, the occurrence of landslides is best predicted using a combination of daily rainfall and 15 days antecedent rainfall. The respective rainfall thresholds has an overall accuracy of 86 %, which is higher than the overall accuracy of the 3, 5, 10, 20 and 30–day thresholds. However, there are several uncertainties inherent in the procedure followed, which, besides rainfall data, are related to the reliability of the landslide date in the inventory. A high degree of uncertainty is also attributed to the selection of non-landslide dates, as some events might have not been reported. Another source of uncertainty is related to the large variability of conditions under which landslides occur within the same area, due to variations in soil depth, slope angle and other characteristics.

The results indicated a spatial and temporal variation of rainfall thresholds in the catchment. The variation of the thresholds for different land uses can be interpreted by the effect of the land cover on the hydrological and mechanical properties of the soil which influence the landslide initiation, for example because of decreased water conductivity due to soil compaction, and slower infiltration rates. On the other hand, the variation of the thresholds at different periods over the year may possibly be due to differences in the type of landslides occurring in these periods (shallow vs deep seated landslides). However, this study did not consider such different types of landslides which according to Muntohar (2008) and Zêzere et al. (2005) can be influenced by different antecedent rainfall conditions. These findings in general suggest that these factors (land cover and period of occurrence) should be taken into consideration when determining rainfall thresholds for the purpose of improving the forecasting of landslides in the area. This approach can eventually help to improve the performance of dynamic LEWS.

CRediT authorship contribution statement

Elias E. Chikalamo: Methodology, Investigation, Formal analysis, Writing - original draft, Visualization. **Olga C. Mavrouli:** Conceptualization, Methodology, Software, Funding acquisition, Supervision, Writing - review & editing. **Janneke Ettema:** Conceptualization, Methodology, Software, Funding acquisition, Supervision, Writing - review & editing. **Cees J. van Westen:** Conceptualization, Methodology, Software, Funding acquisition, Supervision, Writing - review & editing. **Agus S. Muntohar:** Supervision, Writing - review & editing. **Akhyar Mustofa:** Supervision, Writing - review & editing.

Declaration of Competing Interest

The authors declare that they have no known competing financial interests or personal relationships that could have appeared to influence the work reported in this paper.

Acknowledgements

The authors gratefully acknowledge financial support to the first author from the Faculty of Geo-information Science and Earth Observation of the University of Twente, The Netherlands. Further, the authors would like to thank the Geography Department of the Gadjah Mada University for allowing this research to be done in their field laboratory and all the help rendered during field work. The assistance from Universitas Muhammadiyah Yogyakarta and Balai Litbang SABO is also acknowledged.

Appendix A. Supplementary data

Supplementary material related to this article can be found, in the online version, at doi:https://doi.org/10.1016/j.jag.2020.102093.

References

Adji, T.N., Misqi, M., 2010. The distribution of flood hydrograph recession constant for characterization of karst spring and underground river flow components releasing within Gunung Sewu Karst Region. Indones. J. Geogr. XLII (1), 1–15.

Aleotti, P., 2004. A warning system for rainfall-induced shallow failures. Eng. Geol. 73, 247–265. https://doi.org/10.1016/j.enggeo.2004.01.007.

Balling, R.C., Keikhosravi Kiany, M.S., Sen Roy, S., Khoshhal, J., 2016. Trends in extreme precipitation indices in Iran: 1951-2007. Adv. Meteorol. 2016. https://doi.org/10.1155/2016/2456809.

Barla, M., Antolini, I.F., 2016. An integrated methodology for landslides' early warning systems. Landslides 13, 215–228. https://doi.org/10.1007/s10346-015-0563-8.

Baum, R.L., Godt, J.W., 2013. Estimating the timing and location of shallow rainfall-induced landslides using a model for transient, unsaturated infiltration (Journal of Geophysical Research (2010) 115, (F03013) DOI: 10.1029/2009JF001321). J. Geophys. Res. Earth Surf. 118 (3), 1999. https://doi.org/10.1002/jgrf.20100.

Begueria, S., 2006. Validation and evaluation of predictive models in hazard assessment and risk management. Nat. Hazards 37, 315–329. https://doi.org/10.1007/s11069-005-5182-6.

Beguería, S., 2006. Changes in land cover and shallow landslide activity in the Spanish Pyrenees (PDF download Available). Geomorphology 74, 196–206. Retrieved from. https://www.researchgate.net/publication/46667670_Changes_in_land_cover_and_shallow_landslide_activity_in_the_Spanish_Pyrenees.

Berti, M., Martina, M.L.V., Franceschini, S., Pignone, S., Simoni, A., Pizziolo, M., 2012. Probabilistic rainfall thresholds for landslide occurrence using a Bayesian approach. J. Geophys. Res.: Earth Surf. 117 (4), 1–20. https://doi.org/10.1029/2012JF002367.

Berrisford, P., Dee, D., Poli, P., Brugge, R., Fielding, K., Fuentes, M., et al., 2011. The ERA-Interim Archive. Berkshire.

BLS, 2017. SABO Management System. Retrieved February 16, 2018, from. http://sabo.pusair-pu.go.id/new/public/.

BNPB, 2017. BNPB - Badan Nasional Penanggulangan Bencana. Retrieved February 16, 2018, from https://bnpb.go.id/.

Bogaard, T.A., Greco, R., 2016. Landslide hydrology : from hydrology to pore pressure 'L. WIREs Water 3 (June), 439–459. https://doi.org/10.1002/wat2.1126.

Brunetti, M.T., Melillo, M., Peruccacci, S., Ciabatta, L., Brocca, L., 2018. How far are we

from the use of satellite rainfall products in landslide forecasting? Remote Sens. Environ. 210, 65–75. https://doi.org/10.1016/j.rse.2018.03.016.
Bumke, K., 2016. Validation of ERA-interim precipitation estimates over the baltic sea. Atmosphere 7 (6). https://doi.org/10.3390/atmos7060082.
Cepeda, J., Smebye, H., Vangelsten, B., Nadim, F., Muslim, D., 2010. Landslide risk in Indonesia. Global Assessment Report on Disaster Risk Reduction. ISDR Retrieved from. http://www.preventionweb.net/english/hyogo/gar/2011/en/bgdocs/Cepeda_et_al._2010.pdf.
Crozier, M.J., 2010. Deciphering the effect of climate change on landslide activity: a review. Geomorphology 124 (3–4), 260–267. https://doi.org/10.1016/j.geomorph.2010.04.009.
Dowling, C.A., Santi, P.M., 2014. Debris flows and their toll on human life: a global analysis of debris-flow fatalities from 1950 to 2011. Nat. Hazards 71 (1), 203–227.
Farahmand, A., Aghakouchak, A., 2013. A satellite-based global landslide model. Nat. Hazards Earth Syst. Sci. 13 (5), 1259–1267. https://doi.org/10.5194/nhess-13-1259-2013.
Fathani, Faisal, Teuku, Karnawati, D., Fukuoka, H., Honda, K., 2008. Development of Landslide Monitoring and Early Warning System in Indonesia. Retrieved from. http://iplhq.org/wp-content/plugins/file_gmap/130221131129_c9d32224-bf77-4613-bae5-29aca8b3f0ba.pdf.
Fathani, T.F., Karnawati, D., Legono, D., Faris, F., 2011. Development of Eraly Warning System for Rainfall-induced Landslide in Indonesia. Disaster Prevention Research Centre Int Workhsop MSD 2011-Development of early warning system for rainfall-induced landslide in Indonesia.pdf Retrieved from. https://repository.ugm.ac.id/136800/1/2nd.
Gariano, S.L., Guzzetti, F., 2016. Landslides in a changing climate. Earth Sci. Rev. 162, 227–252. https://doi.org/10.1016/j.earscirev.2016.08.011.
Gian, Q.A., Tran, D., Nguyen, D.C., Nhu, V.H., Bui, D.T., 2017. Design and implementation of site-speci fi c rainfall-induced landslide early warning and monitoring system: a case study at Nam Dan landslide (Vietnam). Geomat. Nat. Hazards Risk 8 (2), 1978–1996. https://doi.org/10.1080/19475705.2017.1401561.
Glade, T., Crozier, M., Smith, P., 2000. Applying Probability Determination to Refine Landslide-triggering Rainfall Thresholds Using an Empirical "Antecedent Daily Rainfall Model". Pure Appl. Geophys. 157 (6–8), 1059–1079. https://doi.org/10.1007/s000240050017.
Guzzetti, F., Peruccacci, S., Rossi, M., Stark, P., 2007. Rainfall thresholds for the initiation of landslides in central and southern Europe. Meteorol Atmos Phys. 98, 239–267. https://doi.org/10.1007/s00703-007-0262-7.
Guzzetti, F., Peruccacci, S., Rossi, M., Stark, C.P., 2008. The rainfall intensity-duration control of shallow landslides and debris flows: an update. Landslides. https://doi.org/10.1007/s10346-007-0112-1.
Guzzetti, F., Gariano, S.L., Peruccacci, S., Brunetti, M.T., Marchesini, I., Rossi, M., Melillo, M., 2019. Geographical landslide early warning systems. Earth. Rev., 102973. https://doi.org/10.1016/j.earscirev.2019.102973.
Hadmoko, D.S., Lavigne, F., Sartohadi, J., Gomez, C., Daryono, 2017. Spatio-temporal distribution of landslides in Java and the trigerring factors. Indonesian J. Spatial & Reg. Anal. 31 (1), 1–15. https://doi.org/10.23917/forgeo.v31i1.3790.
Hirnawan, F., 2010. Slope Instability Zoning Mapping of Landslide Hazardous Area for The Stabilization System. Retrieved from. pp. 11–16. https://www.fig.net/resources/proceedings/fig_proceedings/fig2010/papers/fs04d/fs04d_hirnawan_3991.pdf.
Hong, Y., Alder, R., Huffman, G., 2006. Evaluation of the potential of NASA multi-satellite precipitation analysis in global landslide hazard assessment. Geophys. Res. Lett. 33 (22), 1–5. https://doi.org/10.1029/2006GL028010.
Hong, Y., Adler, R.F., Negri, A., Huffman, G.J., 2007a. Flood and Landslide Applications of Near Real-time Satellite Rainfall Products. https://doi.org/10.1007/s11069-006-9106-x.
Hong, Y., Adler, R., Huffman, G., 2007b. Use of satellite remote sensing data in the mapping of global landslide susceptibility. Nat. Hazards 43 (2), 245–256. https://doi.org/10.1007/s11069-006-9104-z.
Hou, A.Y., Kakar, R.K., Neeck, S., Azarbarzin, A.A., Kummerow, C.D., Kojima, M., et al., 2014. The Global Precipitation Measurement Mission. American Meteorological Society, pp. 701–722. https://doi.org/10.1175/BAMS-D-13-00164.1. Retrieved from.
Huffman, G.J., Adler, R.F., Bolvin, D.T., Nelkin, E.J., 2010. The TRMM multi-satellite precipitation analysis (TMPA). In: Gebremichael, M., Hossain, F. (Eds.), Satellite Rainfall Applications for Surface Hydrology. Verlag, Springer, pp. 3–22. https://doi.org/10.1007/978-90-481-2915-7_1.
Huggel, C., Clague, J.J., Korup, O., 2011.). Is climate change responsible for changing landslide activity in high mountains? Earth Surf. Process. Landf. 37 (1), 77–91. https://doi.org/10.1002/esp.2223.
IPCC, 2014. Climate Change 2014 Synthesis Report Summary Chapter for Policymakers 31 Ipcchttps://doi.org/10.1017/CBO9781107415324.
Jian, H., Runqiu, H., Nengpan, J., Qiang, X., Chaoyang, H., 2015. 3D WebGIS-based platform for debris flow early warning: a case study. Eng. Geol. 197, 57–66. https://doi.org/10.1016/j.enggeo.2015.08.013.
Karnawati, D., Fathani, T.F., Andayani, B., Burton, P.W., Sudarno, I., 2009. Strategic program for landslide disaster risk reduction: a lesson learned from Central Java, Indonesia. WIT Trans. Built Environ. 110, 115–161. https://doi.org/10.2495/DMAN090121.
Kidd, C., Dawkins, E., Huffman, G., 2013. Comparison of precipitation derived from the ECMWF operational forecast model and satellite precipitation datasets. J. Hydrometeorol. 14. https://doi.org/10.1175/JHM-D-12-0182.1.
Kirschbaum, D., Kirschbaum, D.B., Huffman, G.J., Adler, R.F., Braun, S., Garrett, K., et al., 2016. NASA'S REMOTELY SENSED PRECIPITATION: A Reservoir for Applications Users. AMS. https://doi.org/10.1175/BAMS-D-15-00296.1.
Kirschbaum, D., Stanley, T., 2018. Satellite-based assessment of rainfall-triggered landslide hazard for situational awareness. Earths Future 6, 505–523. https://doi.org/10.1002/2017EF000715.
Kirschbaum, D.B., Adler, R., Hong, Y., Lerner-Lam, A., 2009. Evaluation of a preliminary satellite-based landslide hazard algorithm using global landslide inventories. Nat. Hazards Earth Syst. Sci. Discuss. 9, 673–686. Retrieved from. www.nat-hazards-earth-syst-sci.net/9/673/2009/.
Kirschbaum, D., Adler, R., Adler, D., Peters-Lidard, C., Huffman, G., 2012. Global distribution of extreme precipitation and high-impact landslides in 2010 relative to previous years. J. Hydrometeorol. 13, 1536–1550. https://doi.org/10.1175/JHM-D-12-02.1.
Kirschbaum, D.B., Stanley, T., Simmons, J., 2015. A dynamic landslide hazard assessment system for Central America and Hispaniola. Nat. Hazards Earth Syst. Sci. 15 (10), 2257–2272. https://doi.org/10.5194/nhess-15-2257-2015.
Lagomarsino, D., Segoni, S., Rosi, A., Rossi, G., Battistini, A., Catani, F., Casagli, N., 2015. Quantitative comparison between two different methodologies to define rainfall thresholds for landslide forecasting. Nat. Hazards Earth Syst. Sci. Discuss. 15, 2413–2423. https://doi.org/10.5194/nhess-15-2413-2015.
Li, X., Zhang, Q., Xu, C.-Y., 2014. Assessing the performance of satellite-based precipitation products and its dependence on topography over Poyang Lake basin. Theor. Appl. Climatol. 115, 713–729. https://doi.org/10.1007/s00704-013-0917-x.
Liao, Z., Hong, Y., Wang, J., Fukuoka, H., Sassa, K., Karnawati, D., Fathani, F., 2010. Prototyping an experimental early warning system for rainfall-induced landslides in Indonesia using satellite remote sensing and geospatial datasets. Landslides 7, 317–324. https://doi.org/10.1007/s10346-010-0219-7.
Ma, T., Li, C., Lu, Z., Wang, B., 2014. An effective antecedent precipitation model derived from the power-law relationship between landslide occurrence and rainfall level. Geomorphology 216, 187–192. https://doi.org/10.1016/j.geomorph.2014.03.033.
Marra, F., Nikolopoulos, E.I., Creutin, J.D., Borga, M., 2014. Radar Rainfall Estimation for the Identification of Debris-flow Occurrence Thresholds. https://doi.org/10.1016/j.jhydrol.2014.09.039.
Martelloni, G., Segoni, I.S., Fanti, I.R., Catani, I.F., 2012. Rainfall thresholds for the forecasting of landslide occurrence at regional scale. Landslides 9, 485–495. https://doi.org/10.1007/s10346-011-0308-2.
Mathew, J., Giri Babu, I.D., Kundu, I.S., Kumar, I.K.V., Pant, I.C.C., 2014. Integrating intensity – duration-based rainfall threshold and antecedent rainfall-based probability estimate towards generating early warning for rainfall-induced landslides in parts of the Garhwal Himalaya, India. Landslides 11, 575–588. https://doi.org/10.1007/s10346-013-0408-2.
Melchiorre, C., Frattini, P., 2012. Modelling probability of rainfallinduced shallow landslides in a changing climate. Clim Chang 113 (2), 413–436.
Melillo, M., Maria, I., Brunetti, T., Peruccacci, S., Gariano, S.L., Guzzetti, F., 2015. An algorithm for the objective reconstruction of rainfall events responsible for landslides. Landslides 12, 311–320. https://doi.org/10.1007/s10346-014-0471-3.
Muntohar, A.S., 2008. Toward regional rainfall threshold for landslide occurrence in Yogyakarta and central of java. J. Tek. Sipil III (1), 1–8.
NASA, 2016. TRMM Mission Overview | Precipitation Measurement Missions. Retrieved December 15, 2017, from https://pmm.nasa.gov/TRMM/mission-overview.
Ngadisih, H., Samodra, G., Bhandary, N.P., Yatabe, R., 2017. Landslide inventory: challenge for landslide hazard assessment in Indonesia. GIS Landslide. https://doi.org/10.1007/978-4-431-54391-6_8.
Nugroho, T., Sadewa, A., Sejati, P., 2014. Identification of groundwater potential zones within an area with various geomorphological units by using several field parameters and a GIS approach in Kulon Progo Regency, Java, Indonesia. Arab J. Geosci. 7, 161–172. https://doi.org/10.1007/s12517-012-0779-z.
Pawestri, M.T., Sujono, J., Istiarto, I., 2017. Flood hazard mapping of Bogowonto River in Purworejo Regency, central java province. J. Civ. Eng. Forum 2 (3), 243. https://doi.org/10.22146/jcef.24348.
Peruccacci, S., Brunetti, M.T., Gariano, S.L., Melillo, M., Rossi, M., Guzzetti, F., 2017. Rainfall thresholds for possible landslide occurrence in Italy. Geomorphology 290, 39–57. https://doi.org/10.1016/j.geomorph.2017.03.031.
Piciullo, L., Calvello, M., Cepeda, J.M., 2018. Territorial early warning systems for rainfall-induced landslides. Earth. Rev. 179, 228–247. https://doi.org/10.1016/j.earscirev.2018.02.013.
Rahmani, V., Hutchinson, S.L., Harrington, J.A., Hutchinson, J.M.S., 2016. Analysis of frequency and magnitude of extreme rainfall events with potential impacts on flooding: a case study from the central United States. Int. J. Climatol. 36 (10), 3578–3587. https://doi.org/10.1002/joc.4577.
Robbins, J.C., 2016. A probabilistic approach for assessing landslide-triggering event rainfall in Papua New Guinea, using TRMM satellite precipitation estimates. J. Hydrolo. 541, 296–309. https://doi.org/10.1016/j.jhydrol.2016.06.052.
Rosi, A., Canavesi, V., Segoni, S., Nery, T.D., Catani, F., Casagli, N., 2019. Landslides in the Mountain Region of Rio de Janeiro : A Proposal for the Semi-Automated Definition of Multiple Rainfall Thresholds.
Rossi, M., Kirschbaum, D., Valigi, D., Mondini, A., Guzzetti, F., 2017. Comparison of satellite rainfall estimates and rain gauge measurements in Italy, and impact on landslide modeling. Climate 5 (4), 90. https://doi.org/10.3390/cli5040090.
Rusdiyatmoko, A., 2013. Incorporating Landslide Susceptibility in Land Rehabilitation. MSc Thesis. University of Twente & Gadjah Mada University.
Segoni, S., Piciullo, L., Gariano, S.L., 2018. A review of the recent literature on rainfall thresholds for landslide occurrence. Landslides 15 (8), 1483–1501.
Sumaryono, Sulaiman, C., Triana, Y.D., Robiana, R., Irawan, W., 2015. Landslide Investigation and Monitoring at Ciloto, West Java, Indonesia. Eng. Geol. Soc. Territory 2, 1089–1096. https://doi.org/10.1007/978-3-319-09057-3_193.
Tan, M., Duan, Z., 2017. Assessment of GPM and TRMM precipitation products over Singapore. Remote Sens. 9 (7), 720. https://doi.org/10.3390/rs9070720.
Tank, A.M.G., Zwiers, F.W., Zhang, X., 2009. Guidelines on Analysis of Extremes in a

Changing Climate in Support of Informed Decisions for Adaptation. Retrieved from last accessed on December 2019. http://www.ecad.eu/documents/WCDMP_72_TD_1500_en_1.pdf.

Teja, T.S., Dikshit, A., 2019. Determination of rainfall thresholds for landslide prediction Using an algorithm-based approach. Case Study in the Darjeeling Himalayas, India, (ID).

Tiranti, D., Rabuffetti, D., 2010. Estimation of rainfall thresholds triggering shallow landslides for an operational warning system implementation. Landslides 7 (4), 471–481. https://doi.org/10.1007/s10346-010-0198-8.

Toté, C., Patricio, D., Boogaard, H., van der Wijngaart, R., Tarnavsky, E., Funk, C., 2015. Evaluation of satellite rainfall estimates for drought and flood monitoring in Mozambique. Remote Sens. 7 (2), 1758–1776. https://doi.org/10.3390/rs70201758.

Turkington, T., Ettema, J., van Westen, C., Breinl, K., 2014. Empirical atmospheric thresholds for debris flows and flash floods in the southern French Alps. Nat. Hazards Earth Syst. Sci. 14, 1517–1530. https://doi.org/10.5194/nhess-14-1517-2014.

Uhlemann, S., Smith, A., Chambers, J., Dixon, N., Dijkstra, T., Haslam, E., et al., 2016. Assessment of ground-based monitoring techniques applied to landslide investigations. Geomorphology 253, 438–451. https://doi.org/10.1016/j.geomorph.2015.10.027.

Ulfa, F., 2017. Debris Flow Susceptibility Analysis Based On Landslide Inventory And Run-Out Modelling In Middle Part Of Kodil Watershed. University of Twente, Central Java, Indonesia MSc Thesis.

UNISDR, 2006. Early Warning Systems in the Context of Disaster Risk Management 29. pp. 2017. from Retrieved May. http://www.ehs.unu.edu/file/get/10735.pdf.

Wehbe, Y., Ghebreyesus, D., Temimi, M., Milewski, A., Mandous, A. Al., 2017. Assessment of the consistency among global precipitation products over the United Arab Emirates. J. Hydrol.: Reg. Stud. https://doi.org/10.1016/j.ejrh.2017.05.002.

Wieczorek, G., Guzzetti, F., 2000. A review of rainfall thresholds for triggering landslides. In: Mediterranean Storms, Proceedings of the EGS Plinius Conference'. 99, (January). pp. 404–414 Retrieved fromhttp://www.idrologia.polito.it/~claps/pliniusonline/pdf_proceedings/Plinius/Wieczorek/WIECZOREK.pdf.

Wu, H., Adler, R.F., Hong, Y., Tian, Y., Policelli, F., 2012. Evaluation of global flood detection using satellite-based rainfall and a hydrologic model. J. Hydrometeorol. 13, 1268–1284. https://doi.org/10.1175/JHM-D-11-087.1.

Yazid, M., Humphries, U., 2015. Regional observed trends in daily rainfall indices of extremes over the Indochina Peninsula from 1960 to 2007. Climate 3 (1), 168–192. https://doi.org/10.3390/cli3010168.

Zêzere, J.L., Trigo, R.M., Trigo, I.F., 2005. Shallow and deep landslides induced by rainfall in the Lisbon region (Portugal): assessment of relationships with the North Atlantic Oscillation. Nat. Hazards Earth Syst. Sci. 5, 331–344. Retrieved from. https://www.nat-hazards-earth-syst-sci.net/5/331/2005/nhess-5-331-2005.pdf.

Zhuang, J., Iqbal, J., Peng, J., Liu, T., 2014. Probability prediction model for landslide occurrences in Xi'an, Shaanxi Province, China. J. Sci. 11 (2), 345–359. https://doi.org/10.1007/s11629-013-2809-z.